HHS Public Access

Author manuscript

J Mech Behav Biomed Mater. Author manuscript; available in PMC 2021 August 06.

Published in final edited form as:

J Mech Behav Biomed Mater. 2017 July ; 71: 397–406. doi:10.1016/j.jmbbm.2017.01.045.

A Hidden Structural Vulnerability in the Thrombospondin-2 Deficient Aorta Increases the Propensity to Intramural Delamination

C. Bellini[1], **N.J. Kristofik**[1], **M.R. Bersi**[1], **T.R. Kyriakides**[1,2,3], **J.D. Humphrey**[1,3]

[1]Department of Biomedical Engineering, Yale University, New Haven, CT

[2]Department of Pathology, Yale School of Medicine, New Haven, CT

[3]Vascular Biology and Therapeutics Program, Yale School of Medicine, New Haven, CT

Abstract

Mice lacking thrombospondin-2 (TSP2) represent an animal model of impaired collagen fibrillogenesis. Collagen constitutes ~1/3 of the wall of the normal murine descending thoracic aorta (DTA) and is thought to confer mechanical strength at high pressures. Microstructural analysis of the DTA from TSP2-null mice revealed irregular and disorganized collagen fibrils in the adventitia and at the interface between the media and adventitia. Yet, biaxial mechanical tests performed under physiologic loading conditions showed that most mechanical metrics, including stress and stiffness, were not different between mutant and control DTAs at 20- and 40-weeks of age, thus suggesting that the absence of TSP2 is well compensated under normal conditions. A detailed bilayered analysis of the wall mechanics predicted, however, that the adventitia of TSP2-null DTAs fails to engage at high pressures, which could render the media vulnerable to mechanical damage. Failure tests confirmed that the pressure at which the DTA ruptures is significantly lower in 20-week-old TSP2-null mice compared to age-matched controls (640±37 vs. 1120±45 mmHg). Moreover, half of the 20-week-old and all 40-week-old mutant DTAs failed by delamination, not rupture. This delamination occurred at the interface between the media and the adventitia, with separation planes often observed at ~45 degrees with respect to the circumferential/axial directions. Combined with the observed microstructural anomalies, our theoreticalexperimental biomechanical results suggest that TSP2-null DTAs are more susceptible to material failure when exposed to high pressures and this vulnerability may result from a reduced resistance to shear loading at the medial/adventitial border.

Keywords

Artery; Stiffness; Strength; Failure; Damage; Dissection

Address for Correspondence: Chiara Bellini, Ph.D., Department of Bioengineering, Northeastern University Boston, MA, 02115 USA, c.bellini@northeastern.edu, +1-617-373-2550.

Conflicts of Interest: none

1. INTRODUCTION

Thrombospondin-2 (TSP2) is a matricellular glycoprotein that modulates interactions between adherent cells and the extracellular matrix (ECM) via a host of cellular receptors, cytokines, growth factors, matrix metalloproteinases (MMPs), and other components of the ECM (Bornstein et al., 2000; Calabro et al., 2014; Yang et al., 2000). Of particular interest here, TSP2 modulates proteolytic activity within the ECM by forming pro- and active MMP2-TSP2 complexes that are bound via the low-density lipoprotein-related receptor protein LRP1, endocytosed, and degraded (Calabro et al., 2014; Yang et al., 2001, 2000). In the absence of TSP2, elevated levels of MMP2 target tissue transglutaminase, which otherwise stabilizes the ECM by promoting isopeptide crosslinks within structural proteins such as collagen and fibronectin (Agah et al., 2005). Hence, although it does not directly associate with collagen, TSP2 plays a critical role in the assembly and arrangement of collagen fibrils and fibers, particularly in load bearing tissues (Calabro et al., 2014). For example, collagen fibers lack proper organization in the skin and tendons of TSP2-null mice, with underlying fibrils being loosely packed with larger than normal diameters and nonuniform cross-sections (Bornstein et al., 2000; Kyriakides et al., 1998). Consequences of such microstructural disorganization include decreased tissue stiffness and mechanical strength, as revealed by uniaxial tensile testing of skin specimens from TSP2-null mice (Kyriakides et al., 1998).

Fibrillar collagen is the main structural constituent of the adventitia, the outermost layer of the aorta, and it is found in lesser amounts within the lamellar units of the media, that is the middle layer. These collagen fibers are thought to contribute significantly to the stiffness of the aortic wall and to dictate its strength. Studies in mice show that diverse mutations that affect the organization of fibrillar collagen adversely affect the biomechanical properties. Mutations to the gene that codes type III procollagen are found in patients affected by one form of Ehlers-Danlos syndrome; they are at risk of sudden death due to arterial rupture. Central arteries from *Col3a1*$^{-/-}$ mice show markedly reduced medial collagen as well as changes in the number and diameter of adventitial collagen fibrils. Most of these mutant mice die before adulthood because of delamination between media and adventitia followed by catastrophic rupture of the aorta (Liu et al., 1997). Mutations to the gene that codes type V collagen result in another form Ehlers-Danlos syndrome, noting that type V collagen contributes to the regulation of collagen fibril nucleation (Wenstrup et al., 2004). Consistent with clinical findings, uniaxial tensile tests on the thoracic aorta of *Col5a1*$^{-/-}$ mice reveal a decreased failure strength (Wenstrup et al., 2006). Biglycan, a small leucine-rich proteoglycan, plays an important regulatory role in the assembly of collagen fibrils. Interestingly, ring tests performed on the aorta of mice deficient in biglycan reveal normal load/strain responses for small deformations, but a significant reduction in the load at rupture (Heegaard et al., 2007). There is, therefore, abundant evidence that diverse mutations that indirectly affect fibrillar collagen compromise the mechanical properties of the aorta.

The effects of TSP2-deficiency on the structural and functional properties of the aortic wall have not been investigated, however. In response to this need, we combined a histological examination (including standard light, polarized light, and transmission electron microscopy) with passive biaxial mechanical and failure testing to assess material properties

of the descending thoracic aorta (DTA) from both TSP2-null and age-matched control mice. Aorta from both young (~20 weeks) and older (40+ weeks) mice were tested to assess the potential of early vascular aging in the absence of TSP2. The data reveal a remarkable ability of the TSP2-null aorta to adapt under physiological conditions and yet an underlying structural vulnerability that manifests at higher distending pressures.

2. EXPERIMENTAL METHODS

2.1 Aortic Specimens.

All animal protocols were approved by the Institutional Animal Care and Use Committee at Yale University. Thrombospondin-2-null (*Thbs2*$^{-/-}$) mice were generated and inbred as described previously (Kyriakides et al., 1998); wild-type (*WT*) mice with a C57BL/6 background were obtained from Jackson Laboratories and used as controls. Blood pressure was measured in alert mice using a standard tail-cuff procedure. TSP2-null mice were euthanized at 20 ($n = 8$) and between 40 and 55 ($n = 5$) weeks of age via a lethal injection of Beuthanasia-D; control mice were euthanized similarly at 20 ($n = 5$) and 40 ($n = 6$) weeks of age. The DTA, between the left subclavian artery and diaphragm, was excised and placed in a Hanks buffered physiological solution (HBSS, Gibco by Thermo Fisher Scientific) at room temperature. Careful removal of loose perivascular tissue exposed the intercostal branches, each of which were ligated with a single thread from a 7–0 braided nylon suture. Vessels were then divided at the second pair of intercostal arteries into proximal and distal specimens, which were used, respectively, for mechanical testing and infusion of elastase to estimate modeling parameters.

2.2 Distension-Extension Tests.

Proximal specimens ($n = 5$ per experimental group) were mounted on custom drawn glass cannulae and secured at each end with ligatures of 6–0 silk suture. They were then submerged in a heated HBSS bath (37°C) and coupled to a custom computer-controlled biaxial device for mechanical testing (Gleason et al., 2004). Following a preliminary estimation of the unloaded geometry (outer diameter and axial length), the vessels were stretched close to their in vivo length, acclimated for 15 minutes while exposed to a pulsatile luminal pressure between 80 and 120 mmHg, and preconditioned with four cycles of pressurization between 10 and 140 mmHg (Ferruzzi et al., 2013). The unloaded geometry was then updated and used to estimate the in vivo axial stretch based on the observed force-pressure behavior (Humphrey et al., 2009; Weizsäcker et al., 1983). Finally, specimens were exposed to three pressure-diameter (*P-d*) protocols, with luminal pressure cycled between 10 and 140 mmHg while axial stretch was maintained fixed at either the in vivo value or ±5% of the in vivo value, and to four axial force-length (*f-l*) tests, with force cycled between 0 and ~40 mN while the luminal pressure was maintained constant at 10, 60, 100, or 140 mmHg (Ferruzzi et al., 2013). Pressure, axial force, outer diameter, and axial length were recorded on-line for all seven protocols for subsequent analysis.

2.3 Failure Tests.

Following these standard distension-extension tests, specimens were remounted on a metal cannula and positioned in a leakage-proof chamber filled with HBSS. The cannula featured

two co-axial, concentric blunt-ended needles of different gauge, which could slide relative to each other to allow luminal pressurization and axial stretching of the vessels (Bersi et al., 2016). Once the unloaded configuration (length and outer diameter) was re-approximated, specimens were stretched to their in vivo axial length and pressurized to failure; luminal pressure and outer diameter were recorded on-line. Failure tests were performed on all specimens that underwent distension-extension tests ($n = 5$ for each of the four experimental groups) as well as on additional specimens for both the *Thbs2*$^{-/-}$ group at 20 weeks ($n = 3$) and the control group at 40 weeks ($n = 1$), where within-group differences in failure were observed. Unloaded wall thickness was measured optically in rings that were cut from either end of the specimens following testing.

2.4 Elastase infusion.

Specimens from the distal DTA ($n = 5$ for each experimental group) were similar to those used for distension-extension tests. After acclimation and preconditioning, the vessels were stretched to their in vivo axial length, pressurized to 100 mmHg, and infused with 3 mL of porcine pancreatic elastase (7.5 U/mL, Worthington Biochemical) for 15 minutes to digest the elastic fibers. Although elastase may have non-specific effects on fibrillar collagens, the primary micromechanical effect is to remove the undulation in the collagen fibers that is induced by the presence of pre-stretched elastic fibers (Ferruzzi et al., 2011). For this reason, measured changes in unloaded length and outer diameter following elastase treatment can be combined with homeostatic values for the biaxial stretches obtained from the distension-extension data to provide a range for the deposition stretches for collagen fibers and smooth muscle needed in the constitutive relations described in Section 3.2 (Bellini et al., 2014), which in turn were used to compute multiple metrics that characterize the biaxial mechanical behavior (cf. Bersi et al., 2016; Roccabianca et al., 2014).

2.5 Histology.

All specimens that underwent mechanical testing (cyclic *P-d* and *f-l* and/or failure) plus additional ($n = 3$ for each of the 4 groups) untested specimens from the proximal DTA were fixed overnight in an unloaded configuration in a 10% neutral buffered formalin solution, then embedded in paraffin and sectioned serially at 5 microns. Vascular cross-sections stained with Verhoeff Van Giesen (VVG), Masson's trichrome (MTC), or picrosirus red (PSR) were imaged with an Olympus BX/51 microscope at 40x magnification. Histological images were processed with a custom MATLAB routine to measure that portion of the wall occupied by media and adventitia as well as to estimate mass fractions for elastin, collagen, and smooth muscle (Bersi et al., 2013).

2.6 Electron Microscopy.

Additional aortas were isolated for transmission electron microscopy (TEM) as described above, except that euthanized animals were perfused with PBS containing 10 U/mL of heparin via gravity flow prior to aortic excision. Isolated vessels were perfusion-fixed with 2.5% glutaraldehyde + 2% paraformaldehyde in 0.1 M sodium cacodylate buffer for regular epon embedding, then placed unloaded in fixative for 30 minutes at room temperature followed by an additional 30 minutes at 4°C. Samples were rinsed in sodium cacodylate buffer before post-fixation in 1% osmium tetraoxide (1 hour), then stained with 2% uranyl

acetate (1 hour) before washing and embedding in epon resin. Sections (60 nm) were collected and viewed on a FEI Technai Biotwin electron microscope.

3. QUANTIFICATION OF MECHANICAL PROPERTIES

Experimental data from cyclic distension-extension tests were used to inform two different constitutive models for the aortic wall. Within the framework of nonlinear anisotropic hyperelasticity, we assumed the existence of a strain energy potential W that defines the elastic energy stored within the material upon deformation; first and second derivatives of W with respect to components of an appropriate measure of deformation yield components of the conjugate measures of stress and stiffness, respectively (Humphrey, 2002). First, following a traditional approach, we modeled the aortic wall as transmurally homogenized and quantified the mean mechanical properties that dictate interactions between the hemodynamics and wall mechanics (Baek et al., 2007). Second, we employed a novel bilayered, constrained mixture model of the aortic wall to obtain layer-specific mechanical properties that are necessary to understand differential responses of the media and adventitia (Bellini et al., 2014; Roccabianca et al., 2014).

3.1 Transmurally-Homogenized Properties and Stress.

The mechanical behavior of the aortic wall was described using a microstructurally-motivated, yet phenomenological, four-fiber family strain energy potential (W), which accounts for the isotropic contribution of an elastin-dominated amorphous matrix and anisotropic contributions due to multiple families of collagen fibers and circumferentiallyoriented passive smooth muscle (Baek et al., 2007; Hu et al., 2007), namely

$$W\left(\mathbf{C},\mathbf{M}^j\right)=\frac{c}{2}(I_{\mathbf{C}}-3)+\sum_{j=1}^{4}\frac{c_1^j}{4c_2^j}\left\{\exp\left[c_2^j\left(IV_{\mathbf{C}}^j-1\right)^2\right]-1\right\}, \tag{1}$$

where c, c_1^j, and c_2^j (j = 1,2,3,4) are model parameters, with c and c_1^j having units of stress (kPa) and c_2^j dimensionless. The right Cauchy-Green deformation tensor $\mathbf{C}=\mathbf{F}^{\mathrm{T}}\mathbf{F}$ was computed from the deformation gradient tensor $\mathbf{F}$, with $det\mathbf{F}=1$ because of assumed incompressibility. The direction of the j^{th} family of fibers was identified by the vector $\mathbf{M}^j=[0,\sin\alpha_0^j,\cos\alpha_0^j]$, with the angle α_0^j expressed with respect to the axial direction in a reference configuration. Based on prior microstructural observations, and the yet unknown effects of copious cross-links amongst the multiple families of fibers, we included contributions of axial ($\alpha_0^1=0$), circumferential ($\alpha_0^2=\pi/2$), and two symmetric diagonal families of fibers ($\alpha_0^{3,4}=\pm\alpha_0$) (Ferruzzi et al., 2013, 2011; Wan et al., 2010). $I_{\mathbf{C}}=tr(\mathbf{C})$ and $IV_{\mathbf{C}}^j=\mathbf{M}^j\cdot\mathbf{C}\mathbf{M}^j$ are coordinate invariant measures of finite deformation. The Cauchy stress tensor $\boldsymbol{\sigma}$ was computed as

$$\boldsymbol{\sigma}=-p\mathbf{I}+2\mathbf{F}\frac{\partial W}{\partial\mathbf{C}}\mathbf{F}^{\mathbf{T}}, \tag{2}$$

where **I** is the second order identity tensor, the superscript T indicates the transpose of the tensor, and p is a Lagrange multiplier that enforces incompressibility. Theoretical values of loads were computed from stress components by solving global equilibrium equations in the radial and axial directions (Humphrey, 2002). Best-fit values for the 8 model parameters in Equation 1 were estimated via nonlinear regression to minimize the sum of the squared differences between the experimentallymeasured and theoretically-predicted values of luminal pressure and axial force, each normalized to the average experimental measures (Ferruzzi et al., 2011; Wan et al., 2010). Estimated parameters (only constrained to be non-negative) were used to predict stored energy, stress, and material stiffness at any configuration. For example, components of the stiffness tensor ($\mathscr{C}_{ijkl}$), linearized about a configuration defined by the mean arterial pressure and in vivo axial stretch, were computed according to (Baek et al., 2007)

$$\mathscr{C}_{ijkl} = 2\delta_{ik}F^o_{lA}F^o_{jB}\frac{\partial W}{\partial C_{AB}} + 2\delta_{jk}F^o_{iA}F^o_{lB}\frac{\partial W}{\partial C_{AB}} + 4F^o_{iA}F^o_{jB}F^o_{kP}F^o_{lQ}\frac{\partial^2 W}{\partial C_{AB}\partial C_{PQ}}\bigg|_{\mathbf{C}^\circ}, \tag{3}$$

where δ_{ij} are components of **I**, $\mathbf{F}^\circ$ is the deformation gradient tensor between the chosen reference configuration and a finitely deformed in vivo configuration, and $\mathbf{C}^\circ$ is the corresponding right Cauchy-Green deformation tensor.

3.2 Layer-Specific Properties and Transmural Stress Distributions.

Unlike the homogenized model, which takes the intact, traction-free configuration of the artery as a reference, our bilayer model of the aortic wall considers the in vivo, homeostatic configuration at mean arterial pressure and in vivo axial stretch as a computationally convenient and physiologically relevant reference configuration (Bellini et al., 2014; Bersi et al., 2016; Cardamone et al., 2009; Roccabianca et al., 2014). Moreover, it assumes the aortic wall is a constrained mixture, with structurally significant constituents (elastindominated amorphous matrix, smooth muscle, and multiple families of collagen fibers) endowed with individual deposition stretches (Humphrey and Rajagopal, 2002), which are defined as the stretch from the natural configuration of each microstructural constituent (i.e., the configuration in which that constituent is stress-free) to the in vivo reference configuration for the mixture (Baek et al., 2006). A rule-of-mixture constitutive formulation was used to obtain the strain energy potential W for the mixture as a weighted sum of the contributions of individual components separately within the media and adventitia (Bellini et al., 2014; Cardamone et al., 2009; Roccabianca et al., 2014; Valentín et al., 2009)

$$W_{media,adventitia} = \phi^e W^e(\mathbf{F}^e) + \phi^m W^m(\lambda^m) + \sum_{j=1}^{4} \phi^{cj} W^{cj}(\lambda^{cj}) \tag{4}$$

where superscripts e, m and c refer to elastin-dominated matrix, smooth muscle, and each of four families of collagen fibers (j = 1,2,3,4); ϕ^i and W^i (i = e, m, c) are mass fractions and strain energy potentials for each microstructural constituent, $\mathbf{F}^e$ is the deformation gradient tensor that describes the deformation of the elastin-dominated ground matrix, and λ^m and

λ^{cj} are stretches experienced by smooth muscle and the j^{th} family of collagen fibers, respectively. Similar to Equation 1, the mechanical response of the elastin-dominated matrix was described by a neo-Hookean potential

$$W^e = \frac{c^e}{2}(I_{\mathbf{C}}e - 3), \tag{5}$$

where c^e is a material parameter having the dimension of stress (kPa), $I_{\mathbf{C}^e} = tr(\mathbf{C}^e)$, $\mathbf{C}^e = \mathbf{F}^{e^{\mathrm{T}}}\mathbf{F}^e$, and $\mathbf{F}^e = \mathbf{F}\mathbf{G}_h^e$, with $\mathbf{G}_h^e$ the deposition stretch tensor. Similar to the homogenized approach, mechanical contributions of smooth muscle and collagen fibers were modeled by Fung-type potentials

$$W^m = \frac{c_1^m}{4c_2^m}\left[e^{c_2^m(IV^m-1)^2} - 1\right], \tag{6}$$

$$W^{cj} = \frac{c_1^c}{4c_2^c}\left[e^{c_2^c(IV^{cj}-1)^2} - 1\right], \tag{7}$$

where c_1^m and c_1^c are model parameters with the dimension of a stress (kPa) while c_2^m and c_2^c are dimensionless. The current model does not delineate contributions of smooth muscle and circumferential collagen fibers within the media, which were combined within a single structural element. The smooth muscle stretch was computed by projecting $\mathbf{C}$ along the cell axis

$$\lambda^m = \sqrt{IV^m} = G_h^m\sqrt{\mathbf{C}:(\mathbf{M}^m \otimes \mathbf{M}^m)}, \tag{8}$$

where G_h^m is the deposition stretch and $\mathbf{M}^m = [0, \sin\alpha_0^m, \cos\alpha_0^m]$ is a unit vector reflecting the orientation of smooth muscle in the reference configuration. Similarly, the stretch imposed on each family of collagen fibers was defined as

$$\lambda^{cj} = \sqrt{IV^{cj}} = \mathrm{G}_h^{cj}\sqrt{\mathbf{C}:(\mathbf{M}^{cj} \otimes \mathbf{M}^{cj})}, \tag{9}$$

where G_h^{cj} is the deposition stretch and $\mathbf{M}^{cj} = \left[0, \sin\alpha_0^{cj}, \cos\alpha_0^{cj}\right]$ is a unit vector in the direction of the j^{th} family of collagen fibers in the reference configuration. Consistent with the stored energy (W), components of the Cauchy stress tensor ($\sigma_{i,j}$) and linearized stiffness (C_{ijkl}) were computed according to Equations (2) and (3), respectively, while deposition stretches (G_h^i) and mass fractions (ϕ^i) determined the deformation experienced by each microstructural constituent and modulated their contribution to the mechanical function. In contrast to the homogenized approach, the value assumed by each mechanical metric depends on radial position in the bilayered model; hence, the integral form of the equilibrium equations was used to compute the theoretical loads needed in the regression algorithm (Humphrey, 2002). Overall 8 parameters were again estimated: 5 material

parameters, the angle of the diagonal collagen fibers (α_0), and two parameters that quantify the proportion of collagen fibers oriented circumferentially or axially (β_ϑ and β_z). Although the same parameters were used to describe the material response of media and adventitia, relative differences in the mass fractions of microstructural constituents resulted in layer-specific mechanical properties. Based on the estimated parameters, transmural distributions of stored energy, stress, and stiffness were predicted for different configurations of the artery.

4. STATISTICAL ANALYSIS

Experimental measurements and derived mechanical metrics are reported as mean ± standard error of the mean (SEM). One-way analysis of variance (ANOVA), followed by Bonferroni post-hoc comparisons in cases of statistical significance, was used to assess differences among the experimental groups. Significance level was set to $p < 0.05$.

5. RESULTS

TSP2-null mice between 40 and 55 weeks of age were grouped together because of similarities in gross appearance, microstructure, and mechanical behavior. Hence, four experimental groups were compared: TSP2-null mice at 20 (*Thbs2*$^{-/-}$ 20 *wk*) and 40+ (*Thbs2*$^{-/-}$ 40 *wk*) weeks of age plus the respective wild-type controls (*WT* 20 *wk* and *WT* 40 *wk*). Body mass (mean ± SEM) was 28.04±6.27 g for TSP2-null mice and 26.69±0.73 for controls at 20 weeks, but 40.10±2.47 g and 34.32±1.21 g at 40 weeks. Mean and systolic arterial pressures were 95±5 and 118±6 mmHg for TSP2-null mice and 107±2 and 127±1 mmHg for control mice at 20 weeks versus 123±6 and 142±8 mmHg for TSP2-null mice and 132±3 and 154±4mmHg for control mice at 40 weeks. Statistical analyses revealed significant differences in mass and mean arterial pressure between TSP2-null mice at 20 and 40 weeks, and in systolic pressure between the two age groups for the controls.

In contrast with control specimens, which appeared opaque when observed under a dissection microscope, DTAs from TSP2-null mice were nearly translucent at both ages and appeared more fragile when handled with microdissection instruments. Nevertheless, the four experimental groups showed overlapping mean *P-d* behaviors at their group-specific in vivo values of axial stretch (Figure 1,A). Two distinct responses were observed in the *f-l* tests at 100 mmHg luminal pressure, however, with data clustering by age not genotype (i.e., 20 weeks vs. 40 weeks, Figure 1,B). Between-group differences in circumferential distensibility fell within the range of within-group variability (Figure 1,C), while TSP2-null and control mice at 40 weeks exhibited reduced axial extensibility compared with mutant and control mice at 20 weeks (Figure 1,D). Similarly, isoenergy contour plots suggested axial stiffening at lower stretches for both TSP2-null and control mice at 40 weeks (Figure 1,E–F). Consistent with mechanical data, VVG- and MTC-stained cross-sections revealed similar morphology between control (Figure 1G–H) and TSP2-null (Figure 1,I–J) aortas, with no obvious defects in the latter.

Table S1 reports best-fit values of the model parameters for the transmurally homogenized (i.e., radially averaged) constitutive relation for each of the four groups based on group-

specific mean datasets. Individual best-fit sets of parameters for each specimen (not shown) led to the bulk mechanical properties summarized in Table S2, together with the average morphological metrics for the unloaded specimens. Aging increased material stiffness in TSP2-null and control mice, with reduced in vivo axial stretches maintaining axial stress nearly constant but similar values of circumferential stretch leading to higher values of circumferential stress (noting the increase in mean arterial pressure from 20 to 40 weeks of age). Although statistical significance was not reached for either age group, TSP2-null aortas were less thick when unloaded and they stretched less circumferentially when pressurized to mean arterial pressure at their in vivo axial stretch. Aside from these two metrics, TSP2-null mice were overall able to compensate for the mutation and they adapted well to their in vivo configuration.

With the purpose of investigating possible layer-specific mechanical differences, the average *P-d* and *f-l* data sets were used to inform our microstructurally-motivated bilayer model of the aortic wall. Analysis of histological images (Table S3) revealed that all four experimental groups contained similar amounts of elastin (30–35% of the wall in the media, 2–5% in the adventitia). Overall collagen mass fractions remained similar in the TSP2-null mice between 20 and 40 weeks (~5% in the media and 28–30% in the adventitia), while changes were seen with aging in control mice (from 6 to 8% in the media and 29 to 21% in the adventitia). Medial smooth muscle also remained similar in 20- and 40-week-old TSP2-null mice (31–33%), but increased with aging in control mice (from 25 to 34%). Morphological changes of unloaded specimens after elastase infusion led to estimates of deposition stretch for circumferential smooth muscle/collagen within the range [1.055,1.065] for TSP2-null mice and [1.060,1.075] for controls. Based on experimental data from the seven different distension-extension protocols, circumferential deposition stretches for elastin were assigned within the range [1.707,1.710] for TSP2-null mice and [1.810,1.998] for controls, while axial deposition stretches were assigned within the range [1.516,1.582] for TSP2-null mice and [1.512,1.570] for controls. Table S4 reports best-fit model parameters for the bilayered analysis for the four experimental groups. Predicted transmural distributions of stress and stiffness in circumferential and axial directions were similar for 20-week-old TSP2-null mice and controls, which confirms that TSP2-null aortas adapt well to physiologic conditions (Figure 2,A–D). Yet, values of circumferential (Figure 2,G) and axial (Figure 2,H) stiffness for TSP2-null aortas rose above control levels at 40 weeks of age even though stresses increased only modestly (Figure 2,E–F), due in part to the slightly lower MAP in the TSP2-null mice. These observations suggested a progressive connection between TSP2 deficiency and material stiffness above physiological pressure.

Hence, the bilayer analysis was used to predict transmural distributions of stress and stiffness in the circumferential direction for the average TSP2-null and control DTAs stretched to their individual in vivo length but subjected to a luminal pressure increasing from systolic to 45% above systolic. Results suggested that circumferential stress and stiffness increase rapidly in the adventitia of the control artery in response to acute increases in blood pressure, which would be expected to protect the media from excessive distension (Figure 2,I,K). In contrast, circumferential stress and stiffness increase with increasing pressure in both the media and adventitia of the TSP2-null aorta, with the two layers almost sharing the load equally at ~210 mmHg (Figure 2,J,L). The latter could render the media

vulnerable to damage. Consistent with numerical predictions of a higher circumferential stiffness at 40 weeks of age in the TSP2-null aortas, a colorimetric analysis of PSR-stained cross sections (Figure 2,M–P) revealed a higher fraction of red collagen fibers and a lower fraction of green, yellow, and orange fibers compared with age-matched controls (Figure 2,Q).

Burst tests were then performed to investigate possible differences in strength between TSP2-null DTAs and controls at both ages. Two distinct failure modes were observed, rupture or delamination. Specimens that ruptured responded to a linearly increasing pressure with a nonlinearly increasing outer diameter, first rapid, then slower, until an axially oriented through-the-wall tear developed, which released the distending fluid and caused a sudden drop in pressure and thus decrease in diameter (Figure 3,A–B). Specimens that delaminated behaved similarly at lower pressures, but experienced a sudden intramural separation at moderate pressures that was captured by the camera as an abrupt increase in outer diameter; the outer diameter remained fairly constant thereafter until the specimen gradually ceased to hold pressure (Figure 3,C–D). Half of the 20-week-old TSP2-null specimens ruptured and half delaminated; all of the 40-week-old TSP2-null delaminated while all control specimens, save one vessel at 40 weeks, ruptured at much higher pressures than for the mutants (Figure 3,E). That is, the average failure pressure (i.e., pressure at which rupture occurred) was ~43% lower in 20-week old TSP2-null mice when compared with the age-matched controls. No significant differences were found in the average delamination pressure between 20 and 40-week-old TSP2-null mice, or in the burst pressure between the two control groups (Table 1). Histological images from specimens that delaminated revealed that the separation occurred at the interface between the media and the adventitia (Figure 3,F–G). TEM analysis of aortas from control and TSP2-null mice allowed a closer examination of the medial-adventitial border and the collagen within the adventitia. The adventitia was different between the two genotypes at 40 weeks: adventitial collagen fibrils in the controls were organized neatly into compartments surrounding fibroblasts, while those in the TSP2-null aortas were less well organized, with fewer compartments (Figure 3,H–I). There were also obvious differences in the collagen fibrils themselves: fibrils were uniform in shape in the controls (Figure 3,H, inset) while they were often irregular in the TSP2-null aortas (Figure 3,I, inset). Finally, amorphous material was detected at the medial/adventitial interface in the mutant aortas (Figure 3, I).

When observed under a dissection microscope, all ruptured specimens presented with an axial tear cutting through the layers of the wall, suggestive of failure due to elevated circumferential stress at high pressures; interestingly, most axial tears originated at or near an intercostal branch (Figure 4,A). For some of the specimens that experienced intramural delamination, the separation between the media and adventitia involved the whole specimen, from ligature to ligature and all around the main axis of the vessel (Figure 4,B). In other cases, injection of India ink into the lumen revealed intramural separation planes that formed an angle of ~45 degrees with the main axis of the vessel (Figure 4,C). Interestingly, in cases of axisymmetric kinematics, material properties, loads, and boundary conditions, the maximum in-plane shear stress (i.e., one-half of the difference between circumferential and axial stresses, which are principal) acts within planes oriented at 45 degrees with respect to circumferential-axial directions at each radial location throughout the wall. For the purpose

of choosing the most appropriate constitutive model to compute failure stresses, we compared the ability of the transmurally homogenized and the bilayered frameworks to predict the *P-d* behavior measured above physiological pressure. Recall that material parameters for both models (Tables S1 and S4) were estimated from distension-extension tests for transmural pressures up to only 140 mmHg, for which they both provided excellent predictions. Nevertheless, the bilayer model alone was able to predict the *P-d* behavior up to pressures close to failure (Figure 4,D).

A bilayered stress analysis was thus performed to predict values of circumferential and axial stress, and by inference the maximum in-plane shear stress, for the 40-week-old TSP2-null and control groups, each at their individual in vivo axial stretch and failure pressure. Because circumferential and axial stresses are predicted in a bilayered model to be discontinuous at the interface between the media and adventitia, the maximum in-plane shear stress is also predicted to be discontinuous (that is, traction continuity applies only to radial components of stress). The differential maximum in-plane shear stresses at the interface between the media and adventitia (Figure 4H) may suggest a situation that could trigger relative motions between the two layers and thereby initiate their separation. In contrast, the circumferential stress responsible for the axial tear in control mice reached ~0.53 MPa in the media and ~7.45 MPa in the adventitia (Figure 4,E), perhaps suggesting that the adventitia fails first in the case of axial tears. In TSP2-null mice, the circumferential stress at failure was a similar ~0.58 MPa in the media but a much lower value of ~2.48 MPa in the adventitia (Figure 4,F), consistent with both a lower burst pressure and a lower strength of the adventitia despite the increase in red fibers in the PSR-stained sections (Figure 2Q). Note that, despite the lower failure pressure in the TSP2-null aortas (415 vs. 1048 mmHg), the media is equally loaded in TSP2-null and control aortas (Figure 4E,F), consistent with the delayed engagement of the mutant collagen fibers (cf. Figure 2,I–J). Given that all 40-week-old TSP2-null vessels failed via delamination, it may be that a circumferential stress equal to or lower than 0.58 MPa does not cause irreparable medial damage. Hence, failure of control vessels may begin with the rupture of the adventitia, after which the load previously supported by the adventitial collagen is transferred to the media, where it leads to catastrophic failure of the elastic laminae and smooth muscle. The predicted maximum in-plane shear stress at the media/adventitia border was 3.86 MPa in the controls, which did not delaminate (Figure 4,G), but only ~0.99 MPa in the TSP2-null vessels, which delaminated (Figure 4,H). Combined with TEM findings (cf. Figure 3,H–I), these results suggest that the irregular and disorganized collagen fibrils in TSP2-null aortas reduces the strength of the adhesion between the media and the adventitia, which may separate at much lower values of in-plane shear stress compared to control vessels.

6. DISCUSSION

Matricellular proteins are thought to contribute to the organization and biomechanical stability of the ECM by modulating cell-matrix interactions and cell signaling rather than by serving directly as structural components (Bornstein et al., 2000). Mice lacking matricellular proteins often present mild phenotypes upon gross examination (Yang et al., 2000), and TSP2-null mice are no exception (Kyriakides et al., 1998). The present study is the first, however, to evaluate possible differences in the structural and mechanical properties of the

aorta in these mice, particularly at elevated pressures. Pressure-diameter and force-length responses of TSP2-null and control DTAs were comparable under physiologic conditions at the same ages in maturity (Figure 1,A–B). Not surprisingly, then, most radially averaged structural and material metrics, evaluated at group-specific mean arterial pressures and in vivo axial lengths, were not different between age-matched mutant and control mice (Table S2). Comparable energy storage across genotypes and ages suggested further that elastic fiber integrity was not compromised by either the TSP2 deficiency or the modest period of aging.

The remarkable ability of TSP2-deficient aortas to adapt under physiological conditions concealed an intrinsic mechanical vulnerability, however, which was only exposed at high pressures. Our bilayered stress analysis suggested that circumferential loads would not be transferred properly from the media to the adventitia in the average TSP2-null aorta at pressures above systolic (Figure 2,I–J). We hypothesized that the lack of TSP2 preferentially renders the adventitia less mechanically competent and therefore unable to protect the media against acute over-distension. Experiments supported this hypothesis. Although half of the specimens within the 20-week old TSP2-null group ruptured the same way as their age-matched controls (via an axial tear, Figure 3,A), their burst pressure was significantly lower (Figure 3,E; Table 1). While not reflective of the normal in vivo condition, these failure tests nevertheless revealed that the lack of TSP2 affects mechanical strength, not normal stiffness.

Importantly, most of the aortas from the TSP2-null mice delaminated, rather than ruptured, when exposed to high pressure (Figure 4, B–C). Delamination of a multilayered composite material may result from either inter-laminar normal stresses triggering the opening and propagation of a crack (mode I) or shear stresses causing relative sliding (mode II) or scissoring (mode III) between two adjacent layers. Since VVG stained cross-sections of delaminated samples did not show any damage to the elastic laminae (Figure 1,I), it seems unlikely that compromised elastin played a role in the greater propensity of the TSP2-null aortas to delaminate. Rather, the observation of delamination planes at 45 degrees with respect to the axial-circumferential directions (Figure 4,C) supports the speculation that TSP2-null mice have a reduced resistance to differential in-plane shears at the interface between the media and adventitia, and that progressive increases in pressure generate a failure-level shearing condition before the circumferential stress damages the adventitia and leads to catastrophic rupture. That in-plane shears could be causative of delamination is supported by a recent study that found a higher resistance of human aortas to out-of-plane than in-plane shearing loads (Sommer et al., 2016). It is also possible, however, that a non-axisymmetric material response, perhaps due to nonuniform distributions of collagen fibers near branch sites, could generate shear stresses in the circumferential-axial plane sufficient to nucleate a delamination that in turn could propagate quickly. Related to this possibility, branches have been suggested as initiation sites for dissecting aortic aneurysms in apolipoprotein E-deficient mice with chronic infusion of angiotensin II (Gavish et al., 2014; Trachet et al., 2015).

Impaired collagen maturation and crosslinking in the absence of TSP2, due to decreased tissue transglutaminase activity and increased availability of MMP2, are thought to be responsible for the reduced mechanical strength observed in the mouse dermis (Kyriakides

et al., 1998). The observed irregular and disorganized collagen fibers at the medial-adventitial border, which are similar in appearance to those described in dermis (Kyriakides et al., 1998), suggest that the same mechanism could be true herein for the thoracic aorta from TSP2-null mice (Figure 3,I). Interestingly, rupture of myocardium has also been reported in TSP2-null mice treated with angiotensin II, which seems to suggest that TSP2-deficiency prevents collagen-mediated reinforcement in response to pressure overload (Schroen et al., 2004). The process of collagen fibril assembly may be set in motion by interactions between a fibril-initiating molecule and a membrane-bound molecule or receptor, which together promote nucleation and unilateral elongation of fibril intermediates; surface modifications of these intermediate constructs support linear and lateral fusion, whereby the growing collagen fibrils increase in diameter and length, with mature fibrils incorporated within the ECM (Wenstrup et al., 2006). Additional types of collagen, matricellular proteins, small leucine-rich proteoglycans, and large proteoglycans participate in different steps of collagen fibrillogenesis and their absence has been linked to defects in content, size, and morphology of collagen fibrils, which can result in tissue fragility (Wenstrup et al., 2004).

As noted earlier, mutations to the genes that code collagens type III and type V as well as the proteoglycan biglycan all lead to aortopathies (Heegaard et al., 2007; Liu et al., 1997; Wenstrup et al., 2006), including a delamination between the media and adventitia that is often followed by catastrophic rupture of the aorta in *Col3a1*$^{-/-}$ mice (Liu et al., 1997). Both the size of the adventitial collagen fibrils and the delamination in these mice are reminiscent of our observations in the TSP2-null mice at supraphysiological pressures. Decorin and lumican, like biglycan, are also small leucine-rich proteoglycans. Arteries of decorin-null mice have not yet been characterized, but their skin shows reduced strength in uniaxial tests to failure (Reed and Iozzo, 2002). Similarly, a decreased failure strength and overall loss of mechanical functionality have been observed in connective tissues from mice lacking lumican, which affects the process of collagen maturation in skin (Chakravarti et al., 1998), tendons (Jepsen et al., 2002), and cornea (Chakravarti et al., 2000). Several other matricellular proteins also contribute to the process of collagen fibril maturation. Deficiency of tenascin-X, which has also been linked to human Ehlers-Danlos syndrome, prevents proper regulation of collagen deposition by dermal fibroblasts and decreases the tensile strength of mouse skin (Mao et al., 2002). Reduction in skin strength was also observed in mice lacking SPARC, which is involved in collagen cross-linking and incorporation within the ECM (Bradshaw et al., 2003). Early studies similarly showed that TSP2 is necessary to achieve adequate microstructural organization and mechanical strength in tissues with high collagen content, such as skin and tendons (Calabro et al., 2014; Kyriakides et al., 1998). It is clear, therefore, that defects in diverse molecules involved in collagen fibrillogenesis can compromise bulk properties; we studied the effects of one such molecule on the biaxial mechanics of the aorta, but effects of others should be studied similarly.

In conclusion, recalling that collagen constitutes ~1/3 of the wall in the thoracic aorta, we used an existing animal model to study the effects of TSP2 deficiency on aortic mechanics. Interestingly, most of the radially averaged metrics used to characterize the biaxial mechanical behavior of central arteries are similar between TSP2-null and control mice under physiological conditions. Nevertheless, a detailed bilayered analysis of the mechanics

of the aortic wall as well as additional theoreticallymotivated experiments revealed that absence of TSP2 reduces the ability of the adventitia to carry high mechanical loads, which decreases the ultimate mechanical strength of the aorta. Failure tests also unveiled a mechanical weakness of the interface between the media and adventitia in TSP2-null mice, which progresses with aging and appears to be responsible for observed delaminations at high pressures. These results reveal that a mechanical vulnerability associated with the deficiency of nonstructural components of the ECM, such as thrombospondin-2, might not be apparent under physiological conditions, where the cells are able to compensate and adapt the ECM. Hence, standard in vivo assessments of stiffness (e.g., pulse wave velocity or distensibility) and similarly standard in vitro biaxial tests within the range of physiological loads are necessary, but not sufficient, to biomechanically phenotype the aorta in the presence of mutations that can affect the structural integrity of the wall. Strategies must be devised to challenge such arteries and evaluate the wall mechanics in terms of mechanical strength and potential failure mechanisms, particularly in cases of uncontrolled hypertension and especially abrupt increases in blood pressure, as, for example, in weight lifting or similar forms of physical exertion that claim the lives of patients susceptible to aortic dissection.

Supplementary Material

Refer to Web version on PubMed Central for supplementary material.

ACKNOWLEDGMENTS

This work was supported, in part, by grants from the NIH (R01 HL105297 and U01 HL116323 to JDH, R01 HL107205 to TRK) and the AHA (pre-doctoral fellowship to NJK).

8. REFERENCES

Agah A, Kyriakides TR, Bornstein P, 2005. Proteolysis of cell-surface tissue transglutaminase by matrix metalloproteinase-2 contributes to the adhesive defect and matrix abnormalities in thrombospondin-2-null fibroblasts and mice. Am. J. Pathol 167, 81–8. doi:10.1016/S0002-9440(10)62955-0 [PubMed: 15972954]

Baek S, Gleason RL, Rajagopal KR, Humphrey JD, 2007. Theory of small on large: Potential utility in computations of fluid-solid interactions in arteries. Comput. Methods Appl. Mech. Eng 196, 3070–3078. doi:10.1016/j.cma.2006.06.018

Baek S, Rajagopal KR, Humphrey JD, 2006. A theoretical model of enlarging intracranial fusiform aneurysms. J. Biomech. Eng 128, 142–149. doi:10.1115/1.2132374 [PubMed: 16532628]

Bellini C, Ferruzzi J, Roccabianca S, Di Martino ES, Humphrey JD, 2014. A microstructurally motivated model of arterial wall mechanics with mechanobiological implications. Ann. Biomed. Eng 42, 488–502. doi:10.1007/s10439-013-0928-x [PubMed: 24197802]

Bersi M, Bellini C, Di Achille P, Humphrey JD, Genovese K, Avril S, 2016. Novel methodology for characterizing regional variations in material properties of murine aortas. J. Biomech. Eng 138, 1–15. doi:10.1115/1.4033674

Bersi MR, Bellini C, Wu J, Montaniel KRC, Harrison DG, Humphrey JD, 2016. Excessive Adventitial Remodeling Leads to Early Aortic Maladaptation in Angiotensin-Induced Hypertension. Hypertension. doi:10.1161/HYPERTENSIONAHA.115.06262

Bersi MR, Collins MJ, Wilson E, Humphrey JD, 2013. Disparate Changes in the Mechanical Properties of Murine Carotid Arteries and Aorta in Response to Chronic Infusion of Angiotensin-II. Int. J. Adv. Eng. Sci. Appl. Math 4, 228–240. doi:10.1007/s12572-012-0052-4 [PubMed: 24944461]

Bornstein P, Armstrong LC, Hankenson KD, Kyriakides TR, Yang Z, 2000. Thrombospondin 2, a matricellular protein with diverse functions. Matrix Biol. 19, 557–568. doi:10.1016/S0945-053X(00)00104-9 [PubMed: 11102746]

Bornstein P, Kyriakides TR, Yang Z, Armstrong LC, Birk DE, 2000. Thrombospondin 2 modulates collagen fibrillogenesis and angiogenesis. J. Investig. Dermatology Symp. Proc 5, 61–66. doi:10.1046/j.1087-0024.2000.00005.x

Bradshaw AD, Puolakkainen P, Wight TN, Helene Sage E, Dasgupta J, Davidson JM, 2003. SPARC-Null Mice Display Abnormalities in the Dermis Characterized by Decreased Collagen Fibril Diameter and Reduced Tensile Strength. J. Invest. Dermatol 120, 949–955. doi:10.1046/j.1523-1747.2003.12241.x [PubMed: 12787119]

Calabro NE, Kristofik NJ, Kyriakides TR, 2014. Thrombospondin-2 and extracellular matrix assembly. Biochim. Biophys. Acta 1840, 2396–402. doi:10.1016/j.bbagen.2014.01.013 [PubMed: 24440155]

Cardamone L, Valentín A, Eberth J, Humphrey J, 2009. Origin of axial prestretch and residual stress in arteries. Biomech. Model. Mechanobiol 8, 431–446. doi:10.1007/s10237-008-0146-x [PubMed: 19123012]

Chakravarti S, Magnuson T, Lass JH, Jepsen KJ, LaMantia C, Carroll H, 1998. Lumican regulates collagen fibril assembly: Skin fragility and corneal opacity in the absence of lumican. J. Cell Biol 141, 1277–1286. doi:10.1083/jcb.141.5.1277 [PubMed: 9606218]

Chakravarti S, Petroll WM, Hassell JR, Jester JV, Lass JH, Paul J, Birk DE, 2000. Corneal opacity in lumican-null mice: Defects in collagen fibril structure and packing in the posterior stroma. Investig. Ophthalmol. Vis. Sci 41, 3365–3373. [PubMed: 11006226]

Duprey A, Trabelsi O, Vola M, Favre J-P, Avril S, 2016. Biaxial rupture properties of ascending thoracic aortic aneurysms. Acta Biomater. 42, 273–285. [PubMed: 27345137]

Ferruzzi J, Bersi MR, Humphrey JD, 2013. Biomechanical phenotyping of central arteries in health and disease: Advantages of and methods for murine models. Ann. Biomed. Eng 41, 1311–1330. doi:10.1007/s10439-013-0799-1 [PubMed: 23549898]

Ferruzzi J, Collins MJ, Yeh AT, Humphrey JD, 2011. Mechanical assessment of elastin integrity in fibrillin-1-deficient carotid arteries: Implications for Marfan syndrome. Cardiovasc. Res 92, 287–295. doi:10.1093/cvr/cvr195 [PubMed: 21730037]

Gavish L, Beeri R, Gilon D, Rubinstein C, Berlatzky Y, Gavish LY, Bulut A, Harlev M, Reissman P, Gertz SD, 2014. Inadequate reinforcement of transmedial disruptions at branch points subtends aortic aneurysm formation in apolipoprotein-E-deficient mice. Cardiovasc. Pathol 23, 152–159. doi:10.1016/j.carpath.2013.12.005 [PubMed: 24480303]

Gleason RL, Gray SP, Wilson E, Humphrey JD, 2004. A multiaxial computer-controlled organ culture and biomechanical device for mouse carotid arteries. J. Biomech. Eng 126, 787–795. doi:10.1115/1.1824130 [PubMed: 15796337]

Heegaard A-M, Corsi A, Danielsen CC, Nielsen KL, Jorgensen HL, Riminucci M, Young MF, Bianco P, 2007. Biglycan Deficiency Causes Spontaneous Aortic Dissection and Rupture in Mice. Circulation 115, 2731–2738. [PubMed: 17502576]

Hu JJ, Baek S, Humphrey JD, 2007. Stress-strain behavior of the passive basilar artery in normotension and hypertension. J. Biomech 40, 2559–2563. doi:10.1016/j.jbiomech.2006.11.007 [PubMed: 17207488]

Humphrey JD, 2002. Cardiovascular Solid Mechanics - Cells, Tissues, and Organs. Springer-Verlag, New York.

Humphrey JD, Eberth JF, Dye WW, Gleason RL, 2009. Fundamental role of axial stress in compensatory adaptations by arteries. J. Biomech 42, 1–8. doi:10.1016/j.jbiomech.2008.11.011 [PubMed: 19070860]

Humphrey JD, Rajagopal KR, 2002. a Constrained Mixture Model for Growth and Remodeling of Soft Tissues. Math. Model. Methods Appl. Sci 12, 407–430. doi:10.1142/S0218202502001714

Jepsen KJ, Wu F, Peragallo JH, Paul J, Roberts L, Ezura Y, Oldberg A, Birk DE, Chakravarti S, 2002. A Syndrome of Joint Laxity and Impaired Tendon Integrity in Lumican- and Fibromodulin-deficient Mice. J. Biol. Chem 277, 35532–35540. doi:10.1074/jbc.M205398200 [PubMed: 12089156]

Kyriakides TR, Zhu YH, Smith LT, Bain SD, Yang Z, Lin MT, Danielson KG, Iozzo RV, LaMarca M, McKinney CE, Ginns EI, Bornstein P, 1998. Mice that lack thrombospondin 2 display connective tissue abnormalities that are associated with disordered collagen fibrillogenesis, an increased vascular density, and a bleeding diathesis. J. Cell Biol 140, 419–430. [PubMed: 9442117]

Lacolley P, Challande P, Boumaza S, Cohuet G, Laurent S, Boutouyrie P, Grimaud J-A, Paulin D, Lamazière J-MD, Li Z, 2001. Mechanical properties and structure of carotid arteries in mice lacking desmin. Cardiovasc. Res 51, 178–187. [PubMed: 11399260]

Liu X, Wu H, Byrne M, Krane S, Jaenisch R, 1997. Type III collagen is crucial for collagen I fibrillogenesis and for normal cardiovascular development. Proc. Natl. Acad. Sci 94, 1852–1856. [PubMed: 9050868]

Louis H, Kakou A, Regnault V, Labat C, Bressenot A, Gao-Li J, Gardner H, Thornton SN, Challande P, Li Z, Lacolley P, 2007. Role of alpha1beta1-integrin in arterial stiffness and angiotensin-induced arterial wall hypertrophy in mice. Am. J. Physiol. Heart Circ. Physiol 293, H2597–604. doi:10.1152/ajpheart.00299.2007 [PubMed: 17660399]

Mao JR, Taylor G, Dean WB, Wagner DR, Afzal V, Lotz JC, Rubin EM, Bristow J, 2002. Tenascin-X deficiency mimics Ehlers-Danlos syndrome in mice through alteration of collagen deposition. Nat Genet 30, 421–425. [PubMed: 11925569]

Osidak MS, Osidak EO, Akhmanova MA, Domogatskaya SPD and A.S., 2015. Fibrillar, Fibril-associated and Basement Membrane Collagens of the Arterial Wall: Architecture, Elasticity and Remodeling Under Stress. Curr. Pharm. Des doi:10.2174/1381612820666141013122906

Reed CC, Iozzo RV, 2002. The role of decorin in collagen fibrillogenesis and skin homeostasis. Glycoconj. J 19, 249–255. doi:10.1023/A:1025383913444 [PubMed: 12975602]

Roccabianca S, Bellini C, Humphrey JD, 2014. Computational modelling suggests good, bad and ugly roles of glycosaminoglycans in arterial wall mechanics and mechanobiology. J. R. Soc. Interface 11, 20140397. doi:10.1098/rsif.2014.0397

Schroen B, Heymans S, Sharma U, Blankesteijn WM, Pokharel S, Cleutjens JPM, Porter JG, Evelo CTA, Duisters R, Van Leeuwen REW, Janssen BJA, Debets JJM, Smits JFM, Daemen MJAP, Crijns HJGM, Bornstein P, Pinto YM, 2004. Thrombospondin-2 is essential for myocardial matrix integrity: Increased expression identifies failure-prone cardiac hypertrophy. Circ. Res 95, 515–522. doi:10.1161/01.RES.0000141019.20332.3e [PubMed: 15284191]

Sommer G, Sherifova S, Oberwalder PJ, Dapunt OE, Ursomanno PA, DeAnda A, Griffith BE, Holzapfel GA, 2016, Mechanical strength of aneurymatic and dissected human thoracic aortas at different shear loading modes. J. Biomech 49, 2374–2382. [PubMed: 26970889]

Trachet B, Fraga-Silva RA, Piersigilli A, Tedgui A, Sordet-Dessimoz J, Astolfo A, Van Der Donckt C, Modregger P, Stampanoni MFM, Segers P, Stergiopulos N, 2015. Dissecting abdominal aortic aneurysm in Ang II-infused mice: Suprarenal branch ruptures and apparent luminal dilatation. Cardiovasc. Res 105, 213–222. doi:10.1093/cvr/cvu257 [PubMed: 25538157]

Valentín A, Cardamone L, Baek S, Humphrey JD, 2009. Complementary vasoactivity and matrix remodelling in arterial adaptations to altered flow and pressure. J. R. Soc. Interface 6, 293–306. doi:10.1098/rsif.2008.0254 [PubMed: 18647735]

Wan W, Yanagisawa H, Gleason RL, 2010. Biomechanical and microstructural properties of common carotid arteries from fibulin-5 null mice. Ann. Biomed. Eng 38, 3605–3617. doi:10.1007/s10439-010-0114-3 [PubMed: 20614245]

Weizsäcker HW, Lambert H, Pascale K, 1983. Analysis of the passive mechanical properties of rat carotid arteries. J. Biomech 16, 703–15. doi:10.1016/0021-9290(83)90080-5 [PubMed: 6643542]

Wenstrup RJ, Florer JB, Brunskill EW, Bell SM, Chervoneva I, Birk DE, 2004. Type V Collagen Controls the Initiation of Collagen Fibril Assembly. J. Biol. Chem 279, 53331–53337. doi:10.1074/jbc.M409622200 [PubMed: 15383546]

Wenstrup RJ, Florer JB, Davidson JM, Phillips CL, Pfeiffer BJ, Menezes DW, Chervoneva I, Birk DE, 2006. Murine Model of the Ehlers-Danlos Syndrome: col5a1 haploinsufficiency disrupts collagen fibril assembly at multiple stages. J. Biol. Chem 281, 12888–12895. doi:10.1074/jbc.M511528200 [PubMed: 16492673]

Yang Z, Kyriakides TR, Bornstein P, 2000. Matricellular proteins as modulators of cell-matrix interactions: adhesive defect in thrombospondin 2-null fibroblasts is a consequence of increased

levels of matrix metalloproteinase-2. Mol. Biol. Cell 11, 3353–64. doi:10.1091/mbc.11.10.3353 [PubMed: 11029041]

Yang Z, Strickland DK, Bornstein P, 2001. Extracellular Matrix Metalloproteinase 2 Levels are Regulated by the Low Density Lipoprotein-related Scavenger Receptor and Thrombospondin 2. J. Biol. Chem 276, 8403–8408. doi:10.1074/jbc.M008925200 [PubMed: 11113133]

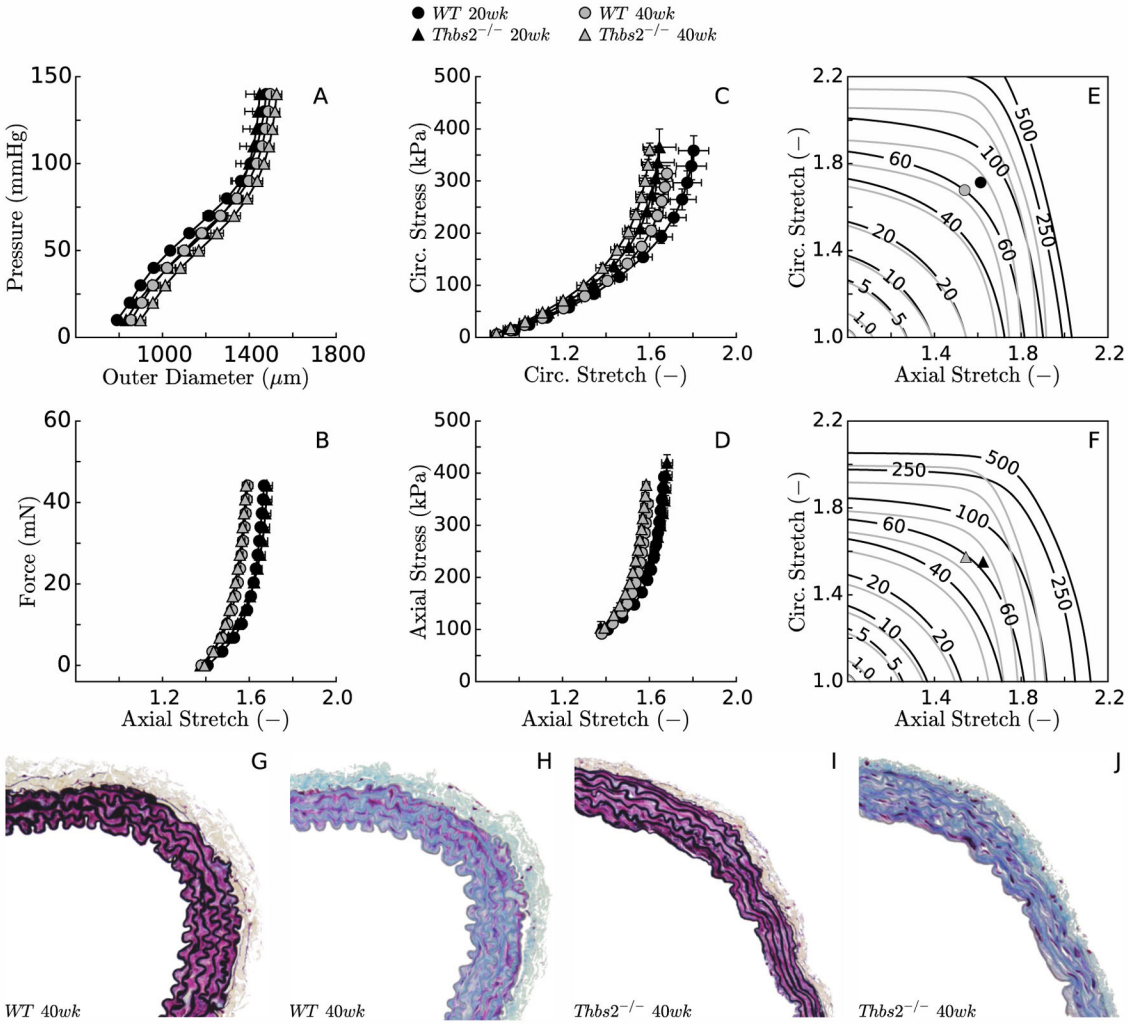

Figure 1.

Biaxial data revealed similar mean structural (panels A-B) and material (panels C-D for stress, and E-F for stored energy, both as a function of stretch) behaviors, independent of the loss of TSP2 at both ages considered (20 and 40 weeks). Aging itself resulted in slight stiffening, however, mainly in the axial direction (panels C-F). Standard light histological examination failed to reveal any obvious difference in fine structure between control (panels G-H, VVG & MTC stains) and TSP2-null (panels I-J, VVG & MTC stains) descending thoracic aortas (DTAs).

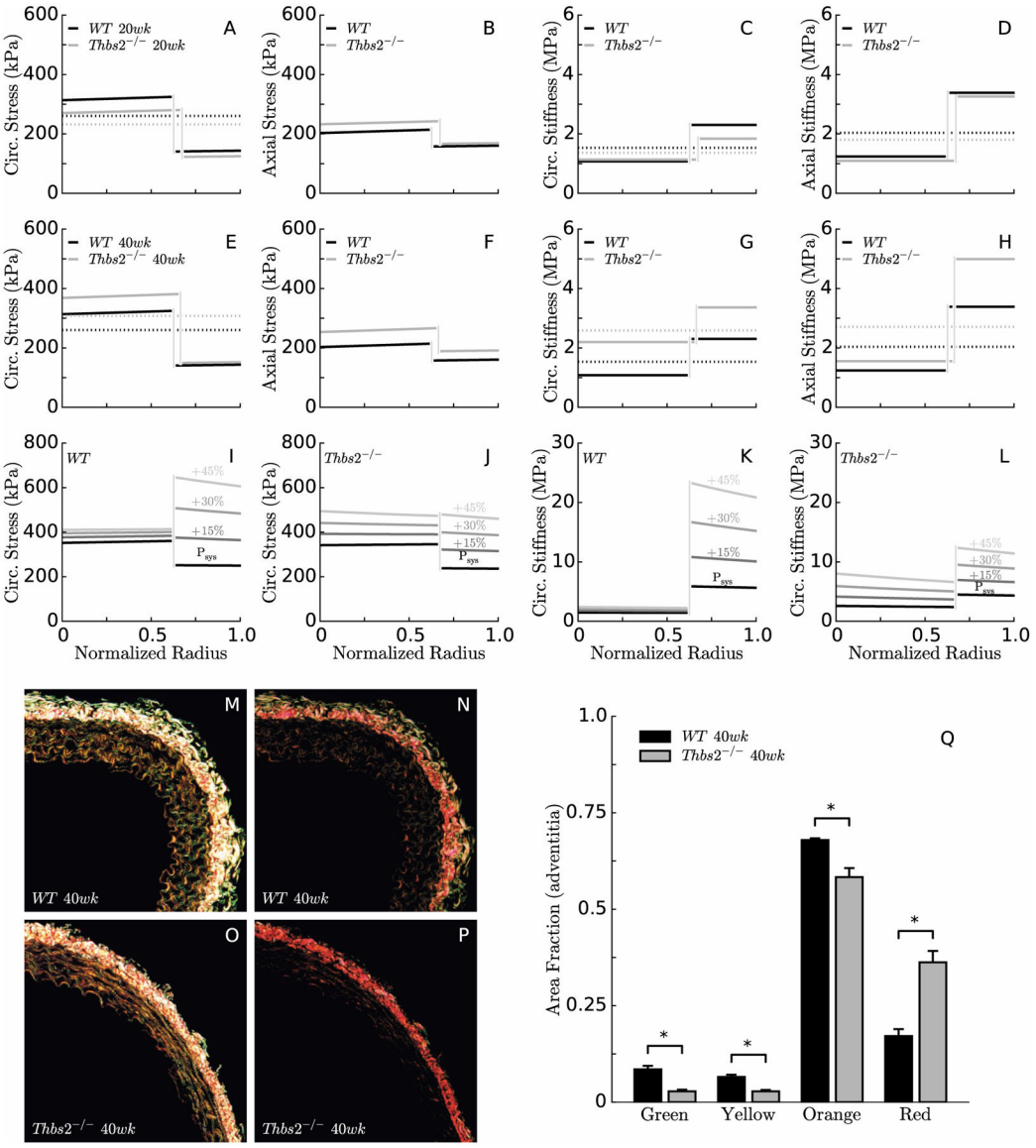

Figure 2.

A bilayered analysis of biaxial wall stress (panels A-B, E-F) and material stiffness (panels C-D, G-H) confirmed that the media carries most of the load in the normal aorta under physiological conditions, which allows medial elastin to store elastic energy. Interestingly, the same is true in TSP2-null aortas. For simulated acute increases in pressure (e.g., 15, 30, or 45% elevations in systolic pressure P_{sys}), the adventitia carries increasingly more load in the normal aorta, thus serving as a protective sheath (panels I,K). In the absence of TSP2, however, the media must bear most of the load since the adventitia fails to provide stress shielding (panels J,L). Consistent with numerical predictions, PSR staining reveals differences in adventitial collagen between *WT* (panels M-N, 400ms & 100ms exposure) and *Thbs2*$^{-/-}$ (panels O-P, 400ms & 100ms exposure) mice; there is a higher content of red collagen fibers and lower content of green, yellow, and orange fibers in the absence of TSP2 at 40 weeks of age. Note that the dotted lines in the circumferential stress plots (panels A, E)

represent the Laplace stress (i.e. the mean value of circumferential stress that comes from the universal solution of a pressurized tube, independent of the specific material response), which serves as a convenient check on the predictions of the bilayered stress analysis. The dotted lines in the linearized stiffness plots (panels C-D, G-H) indicate the integral mean, which can be compared with the average values obtained from the 2-D analysis.

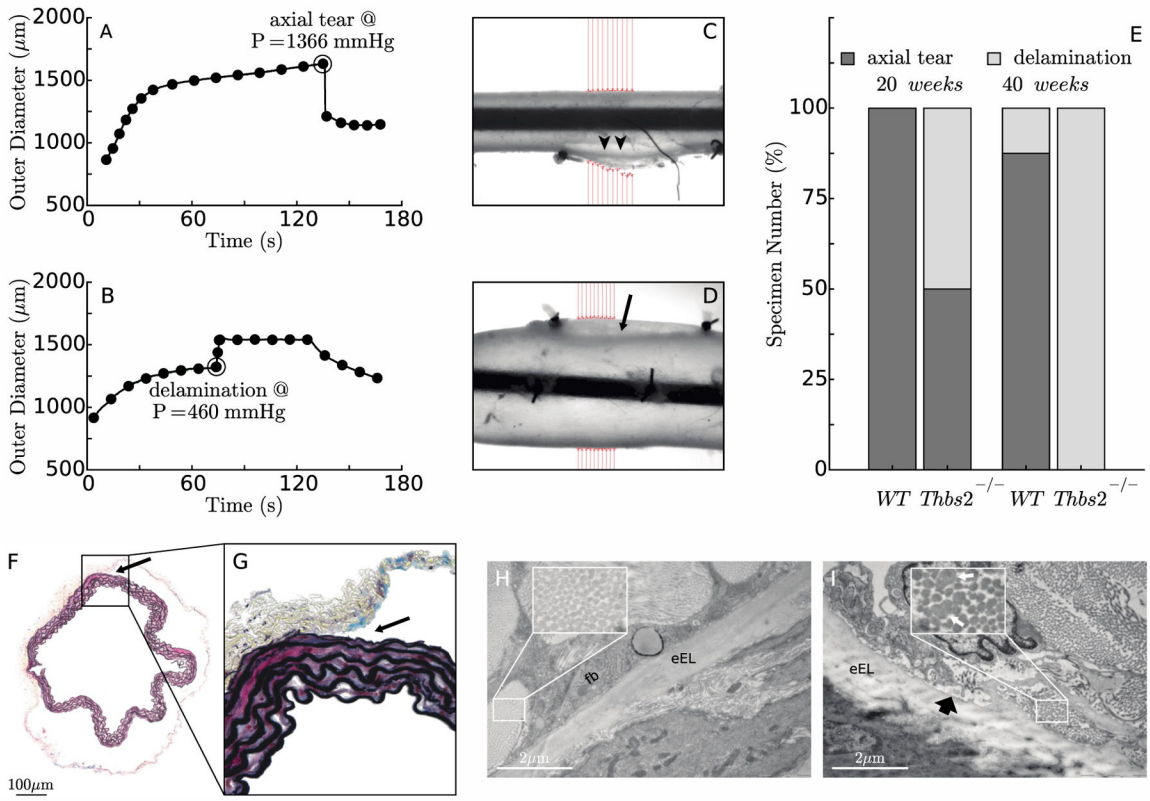

Figure 3:

Two different failure mechanisms – rupture vs. medial-adventitial delamination – were observed in burst pressure tests, not unlike in studies of human aorta (Duprey et al., 2016). The former leads to a sudden loss of pressure-induced circumferential distension (panel A) whereas the latter results in an abrupt increase in outer diameter when the adventitia separates from the media (panel B). Panels C and D show the associated gross failure of two representative aortic specimens mounted within the testing device, with arrowheads showing the location of rupture and the arrow indicating the initiation of a delamination. Panel E reveals the greater age-dependent propensity of TSP2-null aortas to delaminate rather than rupture, which occurred at lower pressures than the rupture events in the controls (panels A-B). Following pressurization to failure, VVG staining of 40-week-old TSP2-null aortas fixed in the unloaded state confirmed that the delamination consistently occurred at the interface between the media and adventitia (panel F). Examination at a higher magnification suggested a clean separation with no damage to the external elastic lamina (panel G). Transmission electron microscopy (TEM) analysis of the media/adventitia interface in intact aortas from 40-week-old mice revealed regular, organized collagen fibrils in *WT* samples (panel H). In contrast, collagen fibrils in *Thbs2*$^{-/-}$ samples were irregular in shape and size (indicated in inset by white arrows) and disorganized (panel I). There also appeared to be more amorphous material at the interface (block, black arrow). eEL denotes external elastic lamina; Fb denotes fibroblast.

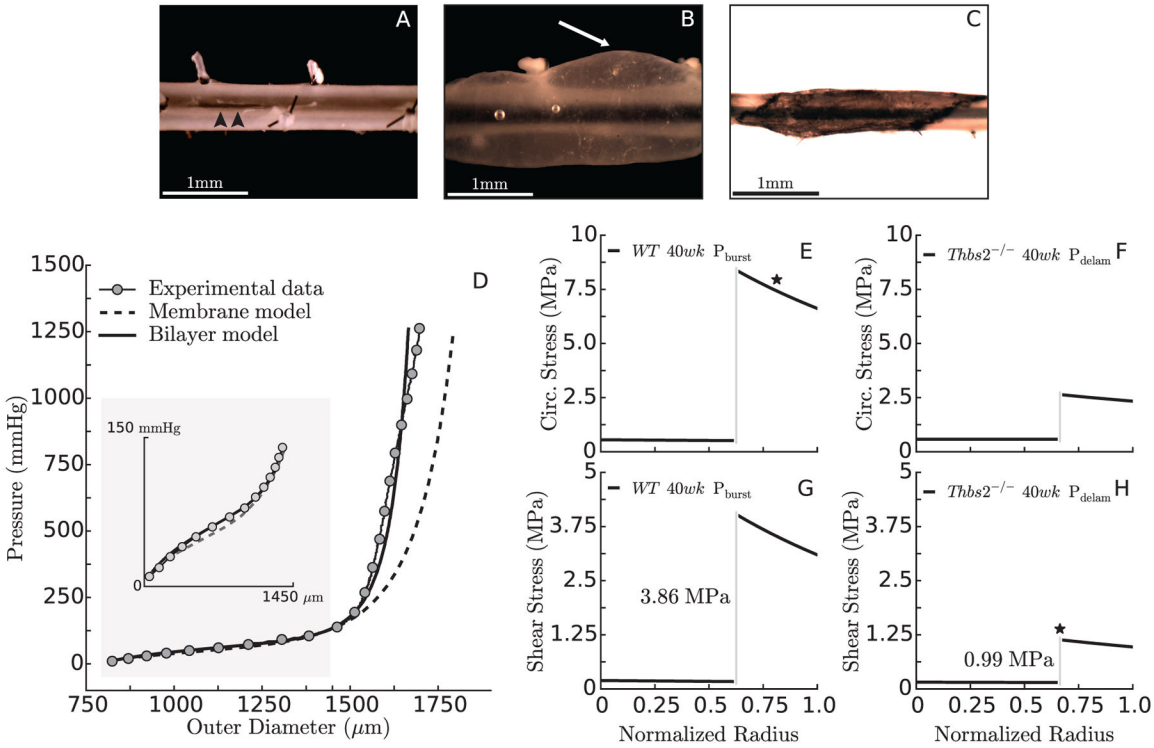

Figure 4:

Ruptured specimens presented with localized through-the-wall axial tears (panel A, arrowheads). In some cases, the delamination spread along the whole specimen (panel B, white arrow) while in others the delamination plane tended to orient at ~45 degrees with respect to the circumferential-axial directions, which was visualized easily following luminal injection of India ink (panel C). In order to choose an appropriate framework for the computation of failure stresses, the ability of the transmurally homogenized and bilayer models to predict the pressure/diameter behavior of the DTA up to failure was compared (panel D). Assuming that elevated circumferential stresses may cause axial tears/rupture (panel A) and in-plane shear stresses may contribute to delaminations (panel B-C), we show bilayer calculations of circumferential (panels E-F) and maximum in-plane shear (panels G-H) stress at the pressure that caused rupture in *WT* (P = 1048 mmHg) or delamination in *Thbs2*$^{-/-}$ (P = 415 mmHg) aortas. The star on the stress plots indicates the presumed stress component associated with mechanical failure (circumferential vs. shear) and the location within the wall where failure appears to initiate (adventitia *vs.* medial/adventitial interface).

Table 1.

Failure pressures (mean ± SEM) for the thoracic aorta from *WT* and *Thbs2*$^{-/-}$ groups at 20 and 40 weeks of age.

	20 weeks		40 weeks	
	WT	***Thbs2*** $^{-/-}$	***WT***	***Thbs2*** $^{-/-}$
n	5	8	6	5
Burst Pressure (mmHg)	1120 ± 45	640 ± 37 *	1048 ± 110	-
Delamination Pressure (mmHg)	-	549 ± 61	585	415 ± 33

* $p < 0.05$ compared to age-matched WT mice (genotype effect)

For comparison purposes, previously reported rupture pressures in common carotid arteries are 1644 ± 54 mmHg for 6–9 month old (Louis et al., 2007) and 2100 ± 80 mmHg for 3 month old (Lacolley et al., 2001) control mice.